Clay Minerals (2021), **56**, 292–298
doi:10.1180/clm.2022.10

CAMBRIDGE UNIVERSITY PRESS

Article

Analysis of tiles produced from a schist material and their ultraviolet, near-infrared, mid-infrared, longwave-infrared and far-infrared spectra

Hulya Kuru Mutlu[1]* and Atakan Mutlu[2]

[1]Eskisehir Osmangazi University, Vocational School of Health Services, Opticianry Program, 26040, Eskisehir, Turkey and [2]Hatipoglu Gunes Tile and Brick Industry, Inc., 43030, Kutahya, Turkey

Abstract

Clays are used in the general production of earthen tiles. In this study, the production and characterization of earthen tiles from schist, a clayey rock formed by metamorphism of mudstone or shale, was investigated. The impact of tiles on atmospheric temperature through their absorption of the visible, near-infrared and far-infrared wavelength regions is evaluated. In particular, the absorption of ultraviolet and infrared radiation by the tiles was evaluated, as this could have beneficial applications for human health and the environment. UV-A radiation (320–400 nm) is not absorbed by the atmosphere, but schist materials absorb UV-A, which can contribute to melanoma formation (i.e. cancer). Field-emission scanning electron microscopy, X-ray fluorescence spectrometry and X-ray diffraction were used for the analysis of the schist materials. The tile-production stages of schist materials (drying, firing, water absorption rate, etc.) were tested at Hatipoglu Gunes Tile and Brick Industry, Inc. (Turkey). The tiles fired at 950°C and 1000°C comply with the industry standard compressive strength values for fired tiles (when converted to industry production conditions) and were 156.15 and 123.20 kg cm^{-2}, respectively.

Keywords: FESEM, industrial application, schist, solar absorption

(Received 20 December 2021; revised 1 March 2022; Accepted Manuscript online: 16 March 2022; Associate Editor: João Labrincha)

Global ceramic coating materials production was 13.26 billion m^2 in 2016, increasing to 13.55 billion m^2 in 2017. Turkey was the eighth highest-producing country of ceramic coating materials, producing 355 million m^2 of ceramic coating materials in 2017 (Cement, Glass, Ceramics and Soil Products Exporters' Association, 2018). Rapid urbanization and rapid population growth have accelerated the growth of the ceramic industry (Ministry of Development T.C., 2015). The selection of raw materials in the tile industry, one of the main subsectors of the ceramic industry, depends on the appearance requirements of the tiles, such as colour and behaviour after firing, which are related to mineralogical and chemical composition and particle-size distribution (Dondi *et al.*, 1999).

An important set of parameters in tile characterization are the optical properties of the tile. Levels of solar reflection of traditional roof coverings have been studied extensively (Berdahl & Bretz, 1997; Bretz & Berdahl, 1997; Prado & Ferreira, 2005). There is insufficient quantitative information on the reflection of solar radiation of most roofing materials, so it is difficult for building designers to select appropriate tile materials. With increasing levels of urbanization, the absorption of solar radiation by tiles is just as important as their reflection of solar radiation.

The wavelength of incoming solar radiation varies between ~300 and 2500 nm. Ultraviolet (UV) radiation consists of radiation with wavelengths <400 nm, while infrared (IR) radiation consists of radiation with wavelengths >800 nm. UV-C (200–280 nm) radiation is absorbed significantly in the atmosphere, while UV-B (280–320 nm) and UV-A (320–400 nm) radiation may reach the Earth's surface. Exposure to UV radiation has negative effects on skin, causing skin cancer, burns, etc. (Barnes *et al.*, 2019). Nevertheless, to our knowledge, the absorption of IR radiation by tiles has not yet been studied. In this study, we report the impacts of tiles, made from schist materials, on the absorption of solar radiation through their absorption of the visible, near-IR (NIR) and far-IR (FIR) wavelength regions.

Previous studies have examined various raw materials in tile production, including quartzite and granite sludges (Torres *et al.*, 2007), epiclastic rocks (Di Gennaro *et al.*, 2007), fly ash (Rajamannan *et al.*, 2007), *tabique* wall samples (Sa *et al.*, 2016), rock dust (Sultana *et al.*, 2015) and ceramic sludges (De Silva & Mallwattha, 2018). Most of these studies have not produced applications for industry because they were performed in laboratory settings and did not perform scaling up of their findings. As an alternative to the clay raw materials, which are frequently used in tile production, schists may also be used. Schists are metamorphic rocks with large particle sizes derived from the metamorphism of mudstones or shales. Schists have been used as alternatives to claystones in cement production (Korkmaz & Hacıfazlıoğlu, 2019). In addition, the usability of schists as filling materials (Korkanç *et al.*, 2017), the mineralogy of schists (Çağatay & Arda, 1979), the properties of slates (schists) (Yagiz, 2011), the colour changes depending on the degree of decomposition of schists (Saroglou *et al.*, 2004) and the optical

*E-mail: hkuru@ogu.edu.tr

Cite this article: Mutlu HK, Mutlu A (2021). Analysis of tiles produced from a schist material and their ultraviolet, near-infrared, mid-infrared, longwave-infrared and far-infrared spectra. *Clay Minerals* **56**, 292–298. https://doi.org/10.1180/clm.2022.10

properties of schists (Afouxenidis *et al.*, 2007) have been studied. As the nature of schists is better established, their use in various industries will increase.

In this study, the chemical, physical and optical properties and industrial usability of schist raw materials in tile production were investigated. The tiles obtained from schists may be suitable for industry, and so their compliance with quality standards was investigated. We report the absorption of the visible, NIR and FIR wavelength regions by tiles made from schist materials. In addition, the properties of the tiles and their absorption of solar radiation were examined. In particular, the tiles' absorption of UV and IR radiation was evaluated, as this could have beneficial applications for human health and the environment.

Materials and methods

The schist used in this study was obtained from the Rızapasa province of Bilecik in Turkey. The working area is located at 39°54'42"N, 30°14'09"E, as determined using a GPSMAP® 60CSx (Garmin, UK).

The mineralogical composition of the schist was determined using X-ray diffraction (XRD) with a Panalytical Empyrean X-ray diffractometer (Malvern, UK). The determination of the mineralogical composition provides important information regarding the raw materials used in production (Bayazit *et al.*, 2020). The chemical composition of the schist was determined using X-ray fluorescence (XRF) spectrometry with a Panalytical Axios Max XRF spectrometer. The particle-size distribution of the schist was examined using dry sieving. All material was passed through a 1 mm sieve. In addition, information regarding the size-distribution ranges and surface topography of the schist was obtained using field-emission scanning electron microscopy (FESEM) with a Regulus 8230 FESEM instrument (Hitachi, Japan).

Humidity levels were determined using a moisture analyser. Small rectangular samples were obtained using a vacuum press device specially produced for Hatipoglu Gunes Tile and Brick Industry by Sermak Makina (Turkey). Samples were dried at 80°C (Ref-San brand, Ceramic Furnaces Industry, Turkey) and then fired in an electric laboratory oven (Ref-San brand, Ceramic Furnaces Industry) at 900°C, 950°C and 1000°C. After firing, the colour, water absorption and compressive strength values of the samples were determined and their compliance with today's TS EN 1304 (2016) standard was evaluated. The calibration of all devices used in tile production was approved by the Turkish Standards Institute.

Fourier-transform IR (FTIR) spectra of the schist tiles were collected using a Bruker Vertex 80v FTIR spectrometer at the Nanoboyut Research Laboratory (Turkey). A Globar-SiC 1100°C source lamp, KBr/deuterated lanthanum α-alanine-doped triglycine sulfate (DLaTGS) D301 detector operating at room temperature and a KBr beam splitter were used in measurements in mid-wave IR (MWIR), long-wave IR (LWIR) and FIR wavelength regions (2.5–25.0 μm). For optical measurements in the NIR (1.0–2.85 μm) wavelength region, background and sample spectra were collected using a tungsten lamp, an indium gallium arsenide (InGaAs) detector and a Ge-CaF_2 beam splitter. Most IR radiation is absorbed by the gases in the atmosphere. For example, radiation with wavelengths of 5.5–7.5 μm is absorbed by H_2O molecules. Therefore, measurements across the whole wavelength range under assessment of 2.5–25 μm were obtained under vacuum.

Results and discussion

The XRD trace of the Rızapasa schist is shown in Fig. 1. The schist consists of chlorite (Ch), albite (Al), mica (M), titanite (Ti). quartz (Q) and actinolite (Ac). Similar mineralogical compositions have been determined in ceramic raw materials (Bayazit *et al.*, 2020; Jordán *et al.*, 2020; Mousavi *et al.*, 2020). Significant increases in tensile strength, hardness and Young's modulus were observed as albite particle content increased (John, 1992; Heinz & Haszler, 2000). The abundance of quartz decreases with increasing firing temperatures of clay materials (Jordán *et al.*, 2020). Heating of albite increases the tensile strength and reduces the softness of ceramics (Doel & Bowen, 1996)

The chemical composition of the Rızapasa schist is listed in Table 1. The main chemical components are SiO_2, Al_2O_3, Fe_2O_3 and CaO. At 700°C, $CaCO_3$ begins to decompose to CaO, accompanied by the evolution of CO_2, and porosity increases. The CaO reacts with the amorphous phase, which is derived from the decomposition of mica at increasing firing temperatures. An increase in water absorption is observed due to the release of CO_2, which increases porosity (Sadik *et al.*, 2013).

The particle-size distribution of the schist sample determined according to ASTM C 136 (2019) is listed in Table 2. The

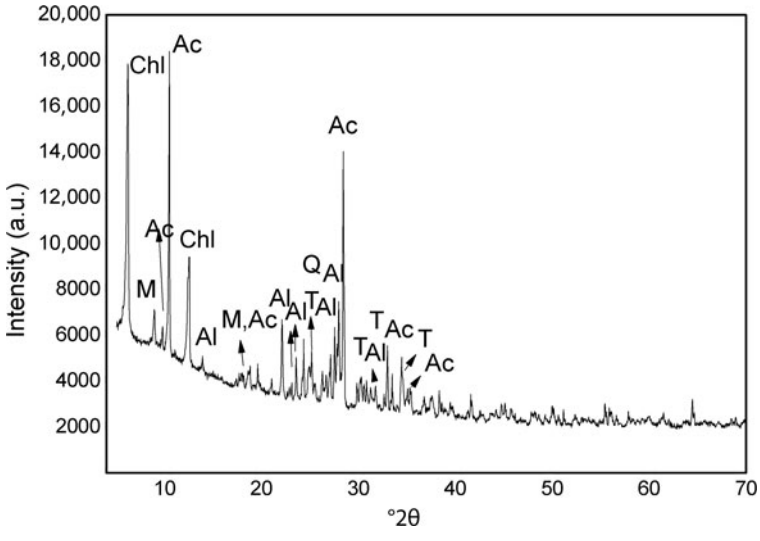

Fig. 1. XRD trace of the Rızapasa schist. Ac = actinolite; Al = albite; Chl = chlorite; M = mica; Q = quartz; T = Al-rich titanite; V = Mg-vermiculite.

https://doi.org/10.1180/clm.2022.10 Published online by Cambridge University Press

Table 1. Chemical composition of the Rızapasa schist determined using XRF spectroscopy.

Component	Tile (%)	Component	Tile (%)
SiO_2	50.51	MgO	1.58
Al_2O_3	9.49	Na_2O	0.11
Fe_2O_3	10.34	K_2O	0.34
TiO_2	2.52	SO_3	0.03
CaO	6.68	LOI	18.40

LOI = loss on ignition.

Table 2. Particle-size distribution of the Rızapasa schist.

Sieve (mm)	Retained (%)
2–4	0
1–2	0
0.05–1	21.00
0.025–0.05	22.67
0.0125–0.025	33.44
0.0062–0.0125	22.21
<0.0062	0.68

proportion of material capable of passing through a 63 µm sieve is 0.68%. The size fraction to be used in tile production includes particles of between 63 and 1000 µm.

The surface topography of the Rızapasa schist sample is shown in Fig. 2. At low magnifications, the sample consists of particles ranging in size from 2.7 to 356 µm (Fig. 2a,b). Observations at higher magnifications reveal the presence of small cracks on the surface. The FESEM analysis shows that the particle size of the schist is suitable for tile production. In a similar study, clays consisting of particles of 200 µm in size produced a glassy phase and pore modification after firing at 995–1150°C (Jordán *et al.*, 2020). Ceramic materials with lower porosity are more resistant to compressive strength (Bressiani *et al.*, 2013; de Oliveira Piccolo *et al.*, 2022).

The moisture content of the schist was 16.73% as measured using the moisture analyser. Test specimens of ~5 cm × 10 cm were prepared by adding the schist and water mixture to a vacuum press device. The physical properties of the samples are listed in Table 3. Drying shrinkage values were determined by recording the physical length measurements (W_i) and weight measurements of the samples (W_e) after drying at 80°C (Table 3). Drying did not produce cracks on the surfaces of the samples (Fig. 3). Samples 1, 2 and 3 were then fired at 900°C, 950°C and 1000°C, respectively, and the influence of firing on compressive strength was recorded. The fired samples (W_f) did not show cracks on their surfaces (Fig. 4). Various firing cycles and transformations as well as particle morphologies are important in the formation of microcracks

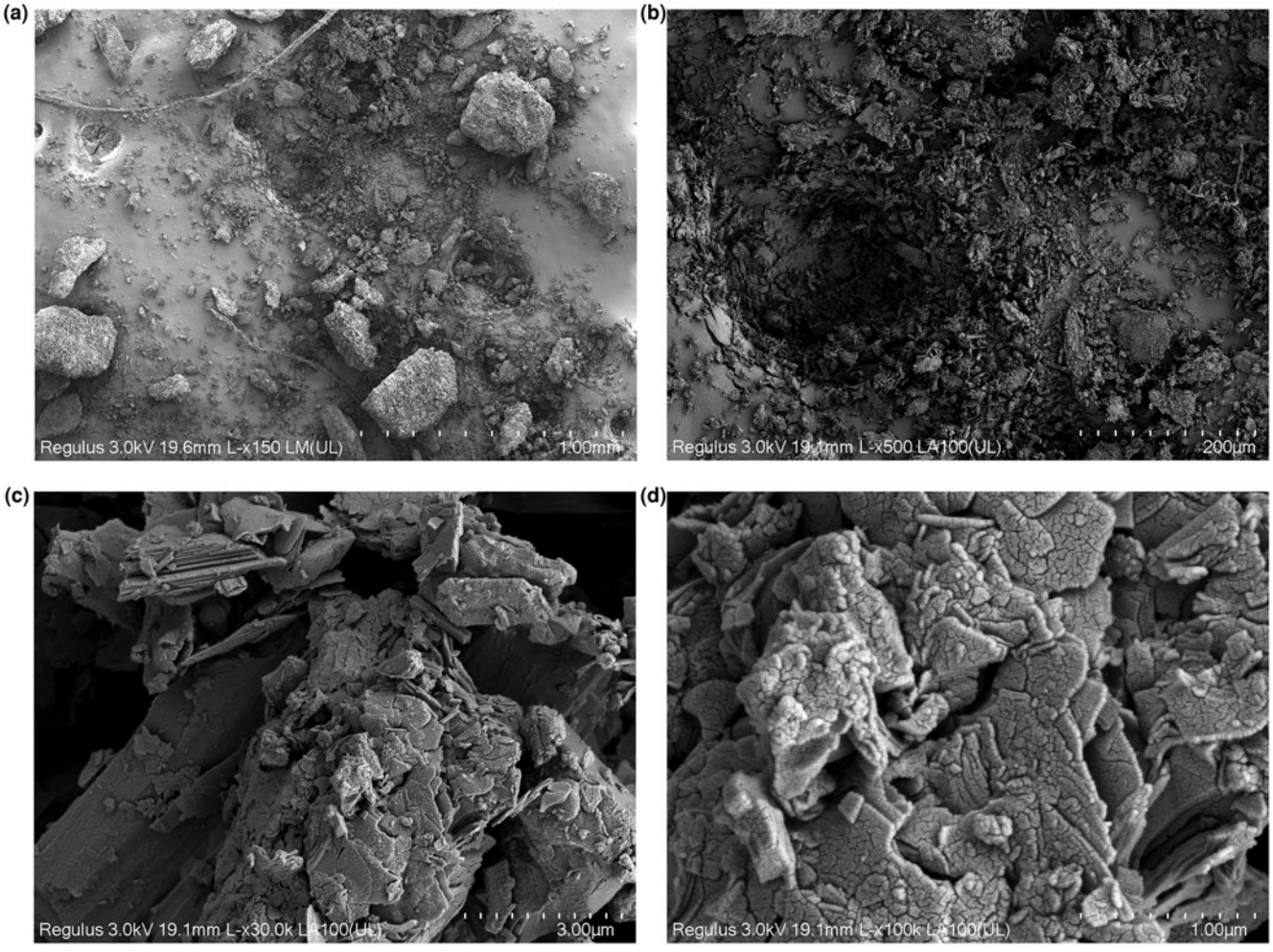

Fig. 2. FESEM images of the Rızapasa schist at (a) 150× magnification, (b) 500× magnification, (c) 30,000× magnification and (d) 100,000× magnification.

https://doi.org/10.1180/clm.2022.10 Published online by Cambridge University Press

Table 3. Shrinkage values of the Rızapasa schist samples after drying and firing.

Dimension	Sample 1	Sample 2	Sample 3
After pressing in a vacuum press device			
Length (mm)	110.00	81.64	128.34
Width (mm)	50.62	50.68	50.31
Weight (g)	219.00	160.0	250.00
After drying			
Length (mm)	109.62	81.37	127.96
Width (mm)	49.87	50.00	49.45
Weight (g)	190.90	138.90	217.70
After firing			
Length (mm)	109.22	80.88	127.66
Width (mm)	49.65	49.85	49.38
Weight (g)	184.00	133.30	208.90

on ceramic structures and in the control of such microcracks (Cabrera *et al.*, 2012; de Oliveira Piccolo *et al.*, 2022).

The drying and firing shrinkage values were calculated according to Equations 1 and 2 (Bacıoglu & Bacıoglu, 2013) and are listed in Table 3.

$$\text{Drying shrinkage} = \frac{(W - W_d)}{W} \times 100\% \quad (1)$$

$$\text{Firing shrinkage} = \frac{(W_d - W_f)}{W_d} \times 100\% \quad (2)$$

From these calculations, the average shrinkage values are given in Table 4.

The samples were placed in water for 24 h to allow the macropores and micropores of the samples to adsorb water (Bureau of Indian Standards, 2002; ASTM C1492, 2003; ASTM C830-00, 2016). Wet (W_w) and dry (W_d) sample weights were recorded and the water absorption rates (W_a) were calculated according to Equation 3 (ASTM C1492, 2003; De Silva & Mallwattha, 2018).

$$W_a = \frac{(W_w - W_d)}{W_d} \times 100\% \quad (3)$$

The schist's average water absorption was calculated as 14.6%. Significant water penetration can lead to the growth of algae, green colouration, etc. Therefore, it is recommended that the water absorption of fired tiles should not exceed 18% (Bureau of Indian Standards, 2002; De Silva & Mallwattha, 2018).

The effects of various firing temperatures on the compressive strength of the schist samples are shown in Table 5. To convert these results to those relevant for industrial production conditions, a conversion factor is used, which, in this case, is the ratio between the compressive strength values used in industry and the compressive strength values used in the laboratory. The converted industry compressive strength values for obtaining tile products from schist raw materials are also listed in Table 5. The breaking load of the furnace tile according to TS EN ISO 10545-4 (2019) and TS EN 1304 (2016) standards should exceed 120 kg m^{-2}. The tiles obtained from schist raw materials meet standard requirements after firing at 950°C and 1000°C. Due to the lack of previous studies on the production of tiles from schists originating from Rızapasa or similar locations, these compressive strength values were compared with those recommended in tile production standards. Topolář *et al.* (2020) placed a mechanical load on a reinforced concrete tile in increments of 5 kN m^{-2}, starting from 10 kN m^{-2} (0.10 kg cm^{-2}). When the mechanical load on the concrete tile reached 35 kN m^{-2}, the stress on the structure increased with further increase of the load. The compressive strength measurements obtained from the schist in the present

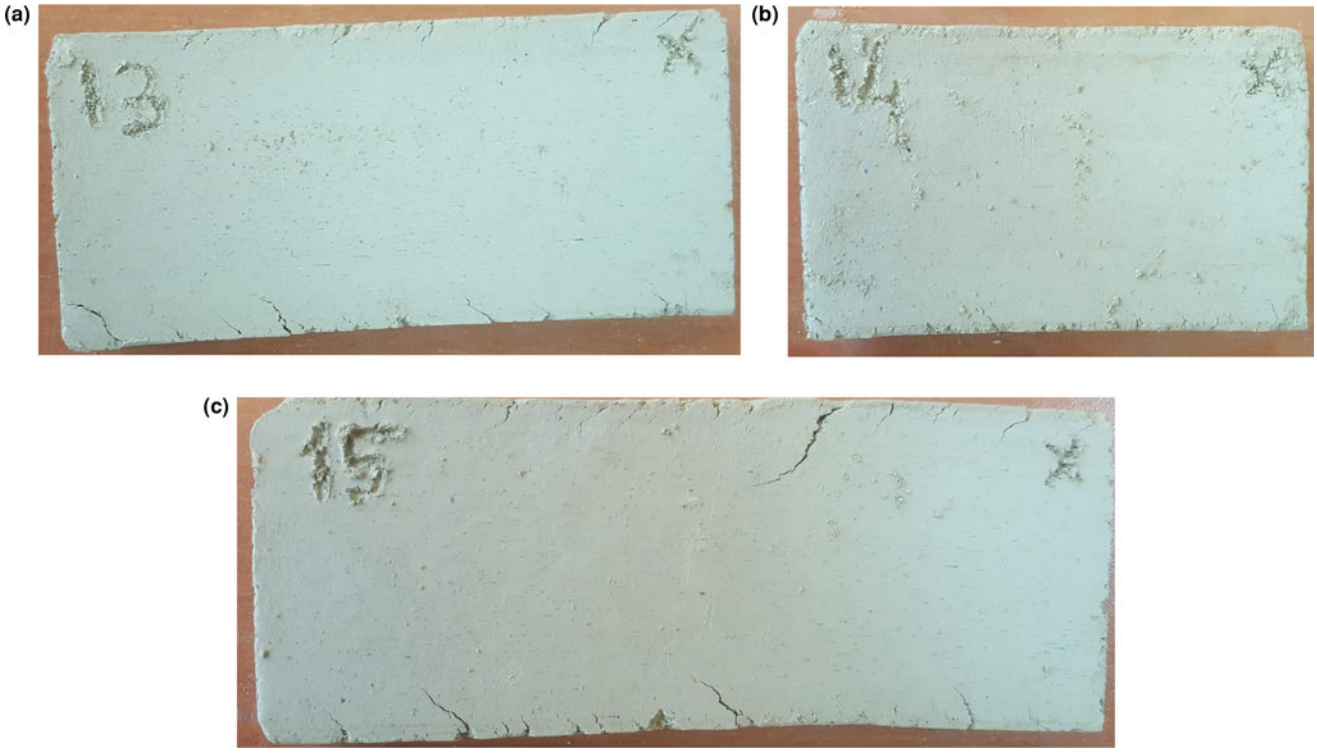

Fig. 3. Photographs of the schist samples after drying. (c) All samples were dried at 80°C.

https://doi.org/10.1180/clm.2022.10 Published online by Cambridge University Press

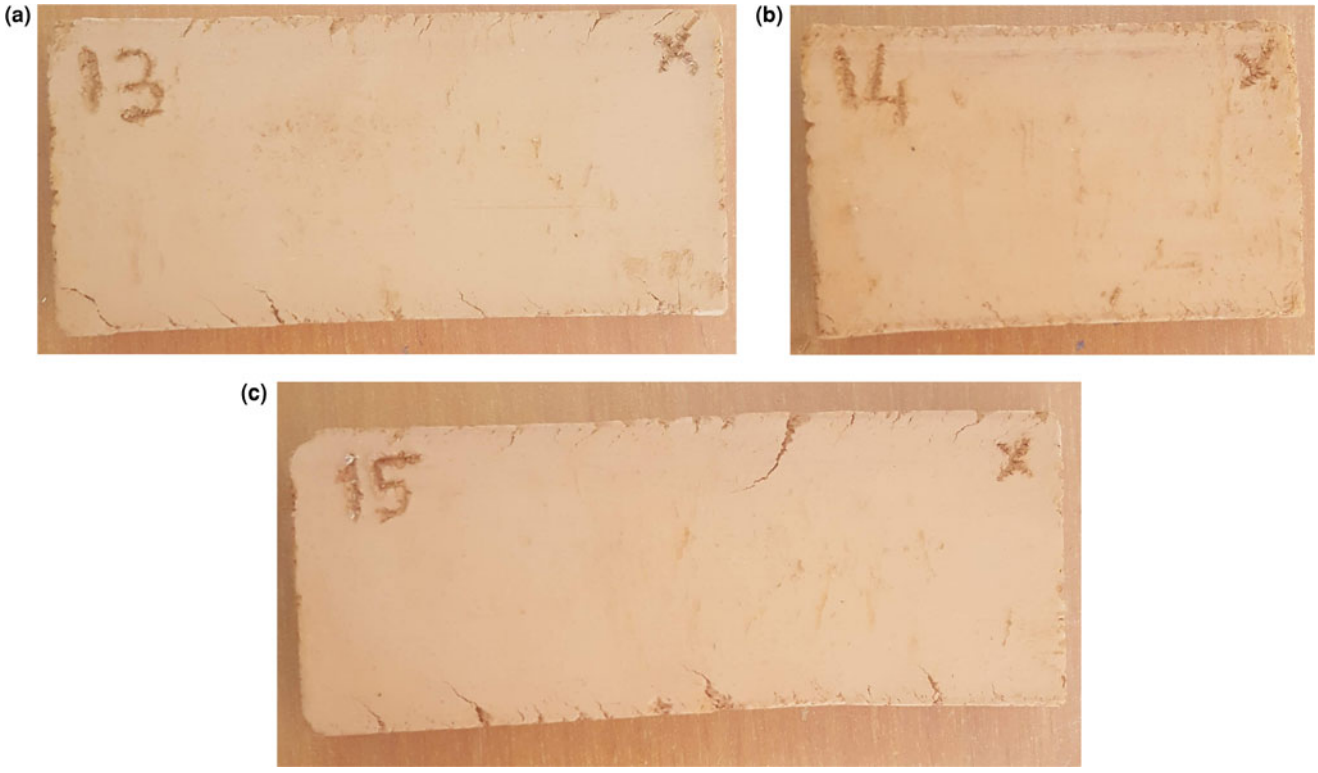

Fig. 4. Photographs of the schist samples after firing at (a) 900°C, (b) 950°C and (c) 1000°C.

Table 4. Average shrinkage values of the Rızapasa schist samples after drying and firing.

Dimension	Shrinkage (%)
Drying shrinkage	
Length	0.0026
Width	0.0146
Weight	0.1293
Firing shrinkage	
Length	0.0036
Width	0.0026
Weight	0.0270

Table 5. Temperature-dependent and converted industry compressive strength values of the Rızapasa schist samples (kg cm^{-2}).

900°C	950°C	1000°C
Compressive strength values		
52.10	68.19	53.80
Converted industry compressive strength values		
119.3	156.2	123.2

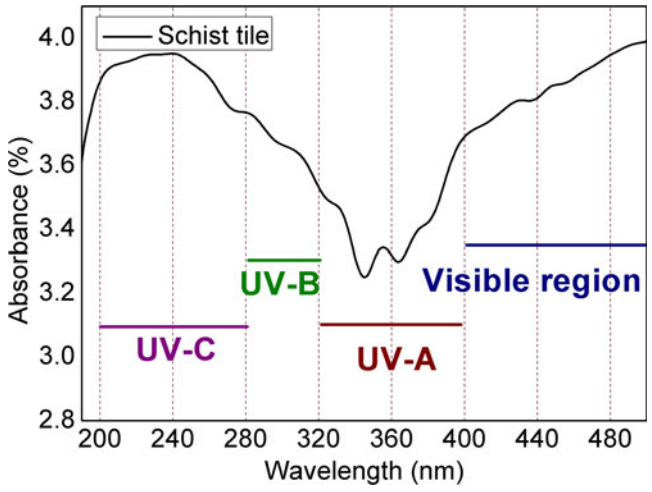

Fig. 5. Absorption of IR radiation by the schist in the UV wavelength region.

study are satisfactory when compared to the compressive strength measurements recorded for red clays (Guimarães *et al.*, 2021).

Due to the fact that clay raw materials have a significant impact on the productivity and the physical, chemical, biological and physicochemical properties of soils, strict regulations make it difficult for mining investors to obtain environmental and zone permits (Ministry of Development T.C., 2015).

The tiles produced from schist materials absorb in the UV wavelength region (Fig. 5). UV-C (200–280 nm) radiation is absorbed significantly in the atmosphere, while UV-B (280–320 nm) and UV-A (320–400 nm) radiation may reach the Earth's surface. In addition, harmful UV-A (320–400 nm) radiation is not absorbed by the atmosphere, but schist materials absorb a portion of UV-A radiation. The effect of exposure to UV-A radiation leading to skin cancer attracted a lot of attention after this was first reported 30 years ago (Setlow *et al.*, 1993). It has since been demonstrated that UV-A radiation has a much more significant impact on the development of melanoma than was understood previously (Wood *et al.*, 2006; Barnes *et al.*, 2019).

The ozone layer absorbs radiation in the NIR wavelength region. Because of its IR radiation absorption, ozone is an

https://doi.org/10.1180/clm.2022.10 Published online by Cambridge University Press

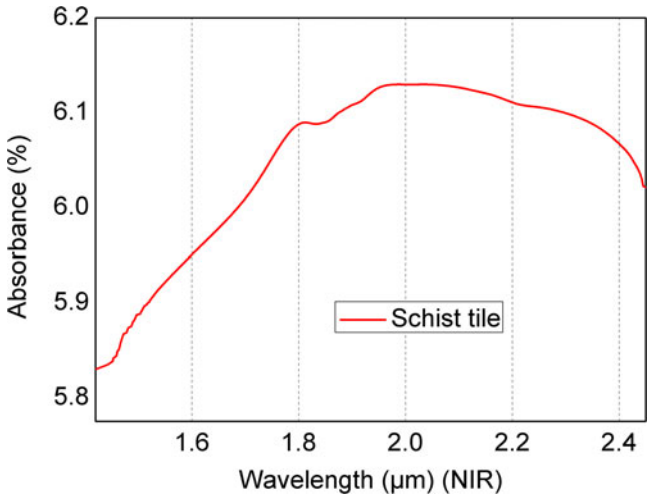

Fig. 6. Absorption of IR radiation by the schist in the NIR wavelength region.

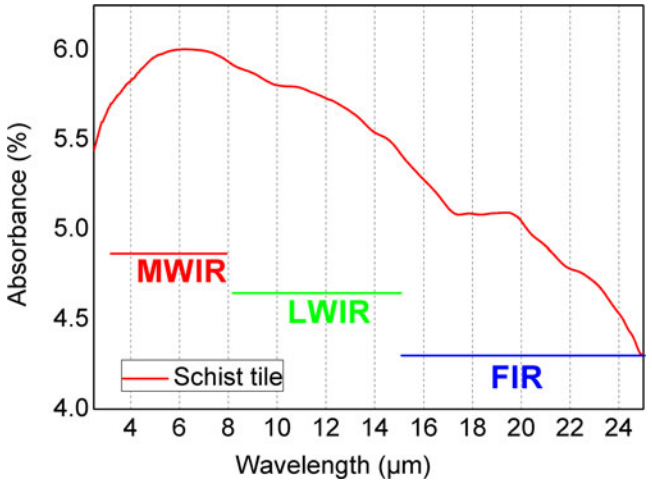

Fig. 7. Absorption of IR radiation by the schist in the MWIR, LWIR and FIR wavelength regions.

important greenhouse gas. When Fig. 6 is examined, it can be seen that the schist tile could contribute to reducing the human-induced greenhouse effect through its absorption of the NIR wavelength region.

The schist tiles absorb in the MWIR, LWIR and FIR wavelength regions (Fig. 7). FIR radiation is a type of radiation that heats objects without heating the air. Apart from heating, it provides many physiological benefits to the human body (Barnes *et al.*, 2019).

Due to the high atmospheric absorption of IR radiation, the experiments in this study were performed under vacuum (Figs 6 and 7).

Conclusions

The Rızapaşa schist, which is used as a raw material in the tile industry, is a useful material for various stages in the tile-production process. The compressive strength values of the samples fired at various temperatures render them suitable for industrial production according to the current industry standard (TS EN 1304, 2016). The level of water absorption was also acceptable. This work is significant due to the lack of studies on the production of tiles from schist materials.

Since the problem of lime explosion on the surface of the tile caused by coarse-grained carbonates is encountered frequently in tiles produced from clays, the introduction of clays into a separator machine to make such products more marketable increases production and transportation costs and thus affects competition in international markets. An important advantage of the Rızapasa schist is that it does not require the use of a separator machine. This reduces production costs.

Environmental pollution arises due to the significant dust emissions that occur when loading raw clay materials onto the transportation vehicles. Such dust can reduce occupational safety and increase occupational diseases. The Rızapasa schist produced much less dust compared to that produced by clays.

The schist tiles in this study absorb harmful UV-A radiation that the ozone layer cannot absorb. In addition to their use in tile production, schist materials are also open to development in many areas such as health due to their absorption in the FIR region of the electromagnetic spectrum.

Acknowledgements. The authors thank Hatipoglu Gunes Tile and Brick Industry, Inc., in Kutahya for the use of their tile production laboratory in this study and Professor Dr Ugur Serincan for the opportunity to take FTIR measurements of the samples at Nanoboyut Research Laboratory, Eskisehir.

Conflict of interest. The authors declare none.

References

Afouxenidis D., Stefanaki E.C., Polymeris G.S., Sakalis A., Tsirliganis N.C. & Kitis G. (2007) TL/OSL properties of natural schist for archaeological dating and retrospective dosimetry. *Nuclear Instruments & Methods in Physics Research Section A: Accelerators, Spectrometers, Detectors and Associated Equipment*, **580**, 705–709.

ASTM C 136 (2019) *Standard Test Method for Sieve Analysis of Fine and Course Aggregates*. ASTM International, West Conshohocken, PA, 5 pp.

ASTM C1492 (2003) *Standard Specification for Concrete Roof Tile*. ASTM International, West Conshohocken, PA, 7 pp.

ASTM C830-00 (2016) *Standard Test Methods for Apparent Porosity, Liquid Absorption, Apparent Specific Gravity, and Bulk Density of Refractory Shapes by Vacuum Pressure*. ASTM International, West Conshohocken, PA, 3 pp.

Bacıoglu A. & Bacıoglu S. (2013) *Tugla ve Kiremit Uretim, Yatırım, İsletme*. Yaman Offset, Ankara, Turkey, 216 pp.

Barnes P.W., Williamson C.E., Lucas R.M., Robinson S.A., Madronich S., Paul N.D. *et al.* (2019) Ozone depletion, ultraviolet radiation, climate change and prospects for a sustainable future. *Nature Sustainability*, **2**, 569–579.

Bayazit M., Adsan M. & Genc E. (2020) Application of spectroscopic, microscopic and thermal techniques in archaeometric investigation of painted pottery from Kuriki (Turkey). *Ceramics International*, **46**, 3695–3707.

Berdahl P. & Bretz S.E. (1997) Preliminary survey of the solar reflectance of cool roofing materials. *Energy and Buildings*, **25**, 149–158.

Bressiani J.C., Genova L.A. & Bressiani A.H.A. (2013) The effect of additives on the microstructure and translucency of alumina. Presented at *96th Annual Meeting of the American Ceramics Society*, Indianapolis, IN, USA, 24–27 April.

Bretz S.E. & Akbari H. (1997) Long-term performance of high-albedo roof coatings. *Energy and Buildings*, **25**, 159–167.

Bureau of Indian Standards (2002) *Clay Roofing tiles, Mangalore Pattern Specification*. Bureau of Indian Standards, New Delhi, 14 pp.

Cabrera M.J., Montins V., Solsona D. & Sala J.M. (2012) Obtención de efectos físico-ópticos para la decoración de baldosas cerámicas. *Boletin de la Sociedad Espanola de Ceramica y Vidrio*, **51**, IX–XVI.

Çağatay A. & Arda O. (1979) The mineralogical studies of schistose rocks occurring in the Bitlis–Yukarı Ölek Köyü–Süllap Bere area with a view about their origin. *Journal of Geological Engineering*, **3**, 55–58.

https://doi.org/10.1180/clm.2022.10 Published online by Cambridge University Press

Cement, Glass, Ceramics and Soil Products Exporters' Association (2018) *Ceramics Industry: Macro Market Research*. Cement, Glass, Ceramics and Soil Products Exporters' Association, Ankara.

de Oliveira Piccolo P., Zaccaron A., Teixeira L.B., de Moraes E.G., Montedo O.R.K., de Oliveira A.P.N. (2022) Development of translucent ceramic tiles from modified porcelain stoneware tile paste. *Journal of Building Engineering, 45*, 103543.

De Silva G.H.M.J.S. & Mallwattha M.P.D.P. (2018) Strength, durability, thermal and run-off properties of fired clay roof tiles incorporated with ceramic sludge. *Construction and Building Materials*, **179**, 390–399.

Di Gennaro R., Dondi M., Cappelletti P., Cerri G., de' Gennaro M., Guarini G. *et al.* (2007) Zeolite-felspar epiclasdtic rocks as flux in ceramic tile manufacturing. *Microporous and Mesoporous Materials*, **105**, 273–278.

Doel T.J.A. & Bowen P. (1996) Tensile properties of particulate-reinforced metal matrix composites. *Composites Part A: Applied Science and Manufacturing*, **27**, 655–665.

Dondi M. (1999) Clay materials for ceramic tiles from the Sassuolo District (Northern Apennines, Italy). Geology, composition and technological properties. *Applied Clay Science*, **15**, 337–366.

Guimarães T.C.D.F., dos Santos A.V., da Cruz Thedoldi A.& de Lima D.C. (2021) Study of the physical and mechanical properties with the chemical composition of red clays from the State of Bahia. *Matéria*, **26**, DOI: 10.1590/S1517-707620210004.1310.

Heinz A. & Haszler A. (2000) Recent developments in aluminum alloys for aerospace applications *Material Science and Engineering A*, **280**, 102–107.

John V.B. (1992) *Introduction to Engineering Materials*. Macmillan Press Ltd, London, 656 pp.

Jordán M.M., Meseguer S., Pardo F. & Montero M.A. (2020) High-temperature mineral formation after firing clay materials associated with mined coal in Teruel (Spain). *Applied Sciences*, **10**, 3114.

Korkanç M., Sener T., Doğan B. & Baskara T. (2017) Geology and building material potential of the Gümüsler-Aktas (Niğde) Region. *Omer Halisdemir University Journal of Engineering Science*, **6**, 132–139.

Korkmaz A.V. & Hacıfazlıoğlu H. (2019) An alternative raw material to clay stone in cement production: meta schist. *Scientific Mining Journal*, **58**, 95–110.

Ministry of Development T.C. (2015) *10th Development Plan 2014–2018*. Ministry of Development T.C., Ankara, 212 pp.

Mousavi S.Z.S., Tavakoli H., Moarefvand P. & Rezaei M. (2020) Micro-structural, petro-graphical and mechanical studies of schist rocks under the freezing–thawing cycles. *Cold Regions Science and Technology*, **174**, 103039.

Prado R.T.A. & Ferreira F.L. (2005) Measurement of albedo and analysis of its influence the surface temperature of building roof materials. *Energy and Buildings*, **37**, 295–300.

Rajamannan B., Sundaram C.K., Viruthagiri G. & Shanmugam N. (2007) Effects of fly ash addition on the mechanical and other properties of ceramic tiles. *International Journal of Latest Research in Science and Technology*, **2**, 486–491.

Sa A.B., Pereira S., Soares N., Pinto J., Lanzinha J.C. & Paiva A. (2016) An approach on the thermal behaviour assessment of *tabique* walls coated with schist tiles: Experimental analysis. *Energy and Buildings*, **117**, 11–19.

Sadik C., El Amrani I.E. & Albizane A. (2013) Effect of andalusite rich schist grain size and the addition of metallic aluminum powder on the properties of silica–alumina refractory. *Journal of Asian Ceramic Societies*, **1**, 351–355.

Sakina B., Imane M., Abdelkader B. & Abdelghani B. (2021) Novel hybrid materials based on montmorillonite-modified reinforced p-phenylenediamine: synthesis, characterization and their optical, electrochemical and thermal properties. *Journal of Molecular Structure*, **1243**, 130866.

Saroglou H., Marinos P. & Tsiambaos G. (2004) Applicability of the Hoek–Brown failure criterion and the effect of the anisotropy on intact rock samples from Athens schist. *Journal of the South African Institute of Mining and Metallurgy*, **104**, 209–215.

Setlow R.B., Grist E., Thompson K. & Woodhead A.D. (1993) Wavelengths effective in induction of malignant-melanoma. *Proceedings of the National Academy of Sciences of the United States of America*, **90**, 6666–6670.

Sultana M.S., Ahmed A.N., Zaman M.N., Rahman M.A., Biswas P.K. & Nandy P.K. (2015) Utilization of hard rock dust with red clay to produce roof tiles. *Journal of Asian Ceramic Societies*, **3**, 22–26.

Topolář L., Kocáb D., Šlanhof J., Schmid P., Daněk P. & Nováček J. (2020) Testing the influence of the material bonding system on the bond strength of large-format tiles installed on concrete substrate under mechanical loading. *Materials*, **13**, 3200.

Torres P., Manjate R.S., Quaresma S., Fernandes H.R. & Ferreira J.M.F. (2007) Development of ceramic floor tile compositions based on quartzite and granite sludges. *Journal of the European Ceramic Society*, **27**, 4649–4655.

TS EN 1304 (2016) Turkısh Standard 2016, clay roofing tiles and fittings – product definitions and specifications. Retrieved from https://intweb.tse.org.tr/Standard/Standard/Standard.aspx?081118051115108051104119110104055047105102120088111043113104073101112105071054115114066067076053#:~:text=Standard%20Detay%C4%B1&text=Kapsam%20%3A,sahip%20olmas%C4%B1%20gerekli%20%C3%B6zelliklerini%20kapsar

TS EN ISO 10545-4 (2019) *Turkey Standard Test Methods for Determination of Modulus of Rupture and Breaking Strength*. Turkish Standards Institution, Ankara, 5 pp.

Wood S.R., Berwick M., Ley R.D., Walter R.B., Setlow R.B. & Timmins G.S. (2006) UV causation of melanoma in *Xiphophorus* is dominated by melanin photosensitized oxidant production. *Proceedings of the National Academy of Sciences of the United States of America*, **103**, 4111–4115.

Yagiz S. (2011) Properties of schist extracted in the city of Denizli surroundings as construction material. *Pamukkale University Journal of Engineering Sciences*, **17**, 157–163.

https://doi.org/10.1180/clm.2022.10 Published online by Cambridge University Press